

VQ-Font: Few-Shot Font Generation with Structure-Aware Enhancement and Quantization

Mingshuai Yao¹, Yabo Zhang¹, Xianhui Lin, Xiaoming Li², Wangmeng Zuo^{1*}

¹ Harbin Institute of Technology

² Nanyang Technological University

{ymsoyosmy,hitzhangyabo2017,xhlin129,csxmli}@gmail.com, wmzuo@hit.edu.cn

Abstract

Few-shot font generation is challenging, as it needs to capture the fine-grained stroke styles from a limited set of reference glyphs, and then transfer to other characters, which are expected to have similar styles. However, due to the diversity and complexity of Chinese font styles, the synthesized glyphs of existing methods usually exhibit visible artifacts, such as missing details and distorted strokes. In this paper, we propose a VQGAN-based framework (*i.e.*, VQ-Font) to enhance glyph fidelity through token prior refinement and structure-aware enhancement. Specifically, we pre-train a VQGAN to encapsulate font token prior within a codebook. Subsequently, VQ-Font refines the synthesized glyphs with the codebook to eliminate the domain gap between synthesized and real-world strokes. Furthermore, our VQ-Font leverages the inherent design of Chinese characters, where structure components such as radicals and character components are combined in specific arrangements, to recalibrate fine-grained styles based on references. This process improves the matching and fusion of styles at the structure level. Both modules collaborate to enhance the fidelity of the generated fonts. Experiments on a collected font dataset show that our VQ-Font outperforms the competing methods both quantitatively and qualitatively, especially in generating challenging styles. Code is available at <https://github.com/Yaomingshuai/VQ-Font>.

1 Introduction

Font library elegantly represents text information in computer systems and has tremendous value in commercial and artistic applications. Manually designing such a library is highly resource-intensive and laborious, especially for logographic languages containing thousands of characters (*e.g.*, Chinese, Japanese, and Korean). However, each glyph is typically constructed using fundamental strokes, thereby making it feasible to create a new glyph by directly adopting styles from other reference glyphs at different levels of granularity, *e.g.*, structure and stroke.

Among these recent methods, few-shot font generation attracts significant attention, as it is effective in reducing the human labor required for designing a target font library. Given limited target glyphs as style references, they usually translate a content glyph to a target one by adaptively

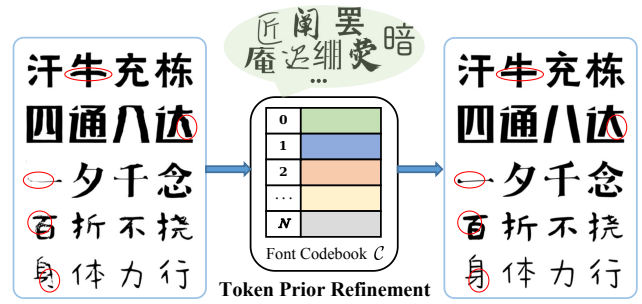


Figure 1: **Left:** The illustration of missing details and distorted strokes, and **Right:** the refinement process through token prior encapsulated in our codebook.

querying fine-grained styles from references. FS-Font (Tang et al. 2022), one of the most representative methods, proposes a style aggregation module based on cross-attention mechanism. It aggregates patch-grained styles to obtain target glyphs. However, it’s noteworthy that the Chinese comprise over 3,000 characters, and subtle variations in strokes can give rise to completely different characters. Besides, nearly all the existing methods learn the representations of characters from scratch, inevitably leading to issues of missing or distorted strokes (see the left part in Fig. 1). Their performance encounters further degradation when handling complex styles, *e.g.*, serif and artistic fonts.

Furthermore, FS-Font takes the patch tokens from content glyphs as queries while those from reference glyphs act as keys and values. This approach focuses on the patch-level correspondence between content and reference glyphs, which neglects the inherent principles of character design. As an ideographic writing system, Chinese characters carry distinct structure information. As shown in Fig. 2, nearly all Chinese characters can be divided into 12 structures, such as top-bottom arrangement and left-right arrangement. Among them, most structures contain two or three components. According to the structure division of Chinese characters, when the radical or character component of the content glyphs appears in the reference glyphs, we aim to treat these structure components as unified entities rather than focusing only on patch-level correspondence.

*Corresponding Author



Figure 2: **Structure component divisions in Chinese characters.** Different colors represent different components.

To improve the fidelity of synthesized glyphs, we propose VQ-Font, a framework encompassing the structure-aware enhancement and token prior refinement. To be specific, we firstly pre-train a VQGAN model (Esser, Rombach, and Ommer 2021) on diverse and high-quality font images. This VQGAN model has the ability to generate font images aligning well with the real-world manifold. Then, we employ a Transformer (Vaswani et al. 2017) to globally model the synthesized font images and predict their corresponding indices within our pre-trained codebook, which can refine the font images by mapping into the token prior space. In addition, we propose a Structure-level Style Enhancement Module (SSEM) to explicitly incorporate Chinese character structure information. By establishing a correspondence between the structure components of the content and reference glyphs, it recalibrates the fine-grained styles derived from the references, thereby facilitating the accurate learning and matching process of glyph style transformation.

In summary, our work has three main contributions:

- We introduce a font codebook that encapsulates token prior to refine synthesized font images. By mapping the synthesized font into the discrete space defined by the codebook, our VQ-Font can effectively address the issues of missing details and distorted strokes.
- We explicitly incorporate the design criterion of Chinese characters by introducing structure-level correspondence. This promotes the model to better learn the styles of the reference glyphs at the structure level.
- Our VQ-Font outperforms these competing methods in both quantitative and qualitative evaluation. It is also capable of generating complex styles with better fidelity.

2 Related Work

2.1 Many-shot Font Generation

Early methods (Tian 2016, 2017; Jiang et al. 2017; Lyu et al. 2017; Chang et al. 2018; Sun, Zhang, and Yang 2018; Jiang et al. 2019; Yang et al. 2019a,b; Gao and Wu 2020; Wu, Yang, and Hsu 2020; Wen et al. 2021; Hassan, Ahmed, and Choi 2021) utilize Image-to-Image translation networks to achieve font generation by learning the mapping function between different fonts. Tian *et al.* presents zi2zi (Tian 2017) which modifies pixel2pixel (Isola et al. 2017) to make it suitable for font generation. AGEN (Lyu et al. 2017) proposes a model for synthesizing Chinese calligraphy images with specified style from standard font images.

HGAN (Chang et al. 2018) proposes a Hierarchical Generative Adversarial Network consisting of a transfer network and hierarchical adversarial discriminator based on zi2zi. PEGAN (Sun, Zhang, and Yang 2018) employs cascaded refinement connections and mirror skip connections to embed a multiscale pyramid of down-sampled input into the encoder feature maps. However, these methods can only transfer glyphs from one known domain to another one that has appeared in the training process, making them incapable of generalizing to new fonts.

2.2 Few-shot Font Generation

In comparison, few-shot font generation is more flexible, as it can obtain a new font library by utilizing a few reference glyphs. Current methods (Sun et al. 2017; Zhang, Zhang, and Cai 2018; Gao et al. 2019; Cha et al. 2020; Park et al. 2021a,b; Xie et al. 2021; Liu et al. 2022; Wang et al. 2023) disentangle font images into content features and style features to achieve few-shot font generation. SA-VAE (Sun et al. 2017), EMD (Zhang, Zhang, and Cai 2018), and AGISNet (Gao et al. 2019) learn global feature representation on font images, but they neglect the design criterion of characters, thereby easily resulting in local details missing. DM-Font (Cha et al. 2020), LF-Font (Park et al. 2021a) and MX-Font (Park et al. 2021b) explicitly decompose characters into components and learn component-wise feature representation to facilitate the learning of local details. XMP-Font (Liu et al. 2022) proposes a self-supervised cross-modality pre-training strategy and a cross-modality transformer-based encoder to model style representation of all scales. DG-Font (Xie et al. 2021) introduces a feature deformation skip connection to predict displacement maps from the content glyph to the target glyph and its improved version, CF-Font (Wang et al. 2023), expands the variety of content fonts and fuses multiple content features by CFM module. Besides, NTF (Fu et al. 2023) achieves few-shot font generation by modeling it as a continuous transformation process using a neural transformation field. Nevertheless, regardless of whether using global or component-wise disentanglement, an average operation is usually performed on the extracted features, which easily weakens the local information and results in the loss of fine-grained details. FS-Font (Tang et al. 2022) begins to avoid explicitly disentangling content and style features of font images. It utilizes a cross-attention mechanism to match the patch-level correspondence between content and reference glyphs, and then aggregate fine-grained styles for font generation. In this work, we mainly follow the settings of FS-Font and attempt to address the issues of missing details and distorted strokes.

2.3 Codebook for Encapsulating Token Prior

VQVAE (Van Den Oord, Vinyals et al. 2017) is an extension of the autoencoder (Hinton and Zemel 1993) that introduces the vector-quantized codebook for the first time. By converting the continuous features into discrete features within a limited space, it resolves the issue of “posterior collapse” in the autoencoder architecture. To achieve better self-reconstruction results, VQVAE2 (Razavi, Van den

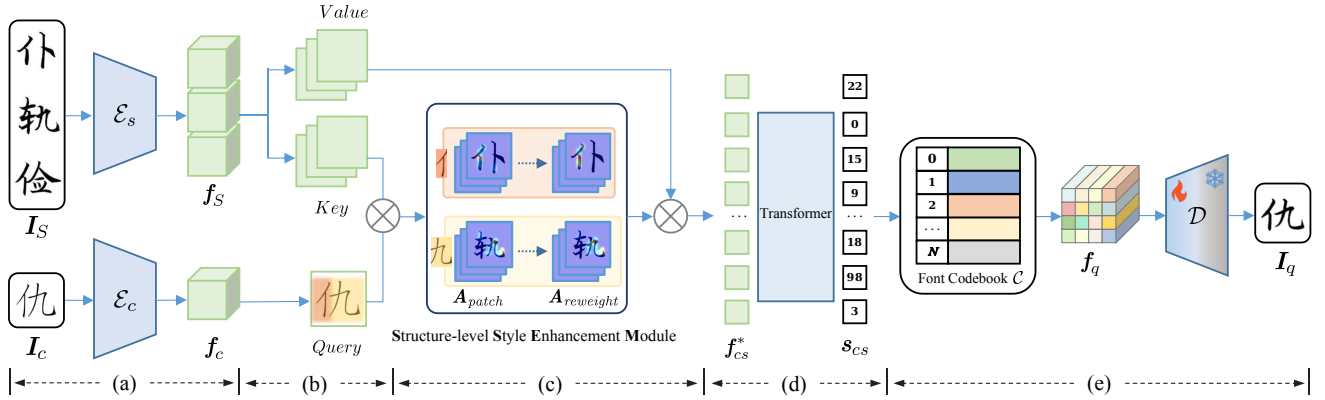


Figure 3: **Overview of VQ-Font framework.** VQ-Font mainly consists of the following components: a style encoder \mathcal{E}_s , a content encoder \mathcal{E}_c , a cross-attention module, a structure-level style enhancement module, a Transformer module, a pre-trained font codebook \mathcal{C} and font decoder \mathcal{D} . (a) \mathcal{E}_s and \mathcal{E}_c first map I_S and I_c into style features f_S and content feature f_c , respectively. (b) Then the cross-attention module is used to learn patch-level attention A_{patch} between the patches of content and references. (c) The structure-level style enhancement module further utilizes the structure information of Chinese characters to reweight A_{patch} , in order to better learn the structure-level styles. (d) The Transformer module models the font images and predicts the target glyph indices s_{cs} . (e) The obtained codebook indices s_{cs} is used to retrieve quantized token vectors from the font codebook, which is subsequently taken into the font decoder to generate the final image.

Oord, and Vinyals 2019) introduces a multi-scale codebook. VQGAN (Esser, Rombach, and Ommer 2021) enhances generation capabilities and further compresses the codebook size by introducing adversarial loss and perceptual loss. During the training phase, the codebook is continuously updated, thus encapsulating rich priors. Currently, the codebook has been used for many image restoration tasks to recover image details. RIDCP (Wu et al. 2023) utilizes a codebook that stores scene graphs without fog/rain information to achieve image dehazing, FeMaSR (Chen et al. 2022) utilizes a high-resolution prior codebook to achieve image super-resolution, Codeformer (Zhou et al. 2022) and VQFR (Gu et al. 2022) utilize a codebook that stores high-quality facial textures for blind face restoration. MARCONet (Li, Zuo, and Loy 2023) combines the codebook and StyleGAN (Karras et al. 2020) to generate the specific characters for providing detailed reference in text image super-resolution tasks. With the aid of the codebook which possesses rich priors, degraded images can be well restored to photo-realistic results. Currently, few-shot font generation tasks also suffer from stroke distortion, detail loss, and other related issues. Inspired by the benefits brought by VQGAN on the aforementioned methods, we introduce a font codebook with rich stroke priors for the first time. By using Transformer (Vaswani et al. 2017) to match corresponding code indices, the re-arranged tokens from the codebook can generate font images with clear strokes and realistic details.

3 Method

Few-shot font generation transfers a content glyph I_c to a new style described by several glyphs $I_S = \{I_s^i\}_{i=1}^k$. It requires ensuring both the quality of synthesized glyphs and the fidelity of captured styles. In this section, we introduce a VQGAN-based framework (i.e., VQ-Font) to improve them through token prior refinement and structure-level style en-

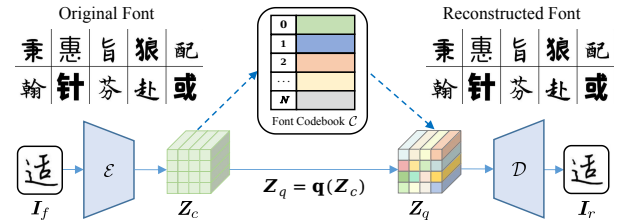


Figure 4: **The details of our font VQGAN.** The encoder \mathcal{E} first maps the font image I_f into continuous feature space Z_c . Then, Z_c is quantized into discrete feature Z_q with font codebook \mathcal{C} . Finally, the decoder maps Z_q back into the image space to generate result I_r . Notably, the *out-of-domain* font can be also well reconstructed using the font VQGAN.

hancement. Firstly, VQ-Font encapsulates stroke priors by VQGAN-based self-reconstruction (Sec. 3.1), and then refines the synthesized strokes with the encapsulated priors (Sec. 3.2). Secondly, it enhances the fine-grained styles using the inherent structure of Chinese characters (Sec. 3.3). The overall training objectives are summarized in Sec. 3.4.

3.1 Self-Reconstruction for Font Token Prior

To learn the token prior and incorporate it into the synthesized fonts, we pre-train a VQGAN by self-reconstructing font images with diverse styles and high quality. As shown in Fig. 4, VQGAN consists of an encoder \mathcal{E} , a learnable codebook $\mathcal{C} = \{c_k \in \mathbb{R}^d\}_{k=1}^K$, and a decoder \mathcal{D} . During self-reconstruction, \mathcal{E} encodes a glyph image $I_f \in \mathbb{R}^{H \times W \times 1}$ into continuous features $Z_c \in \mathbb{R}^{h \times w \times d}$. Then, an element-wise quantization $\mathbf{q}(\cdot)$ is performed to replace each code in Z_c with its closest entry in codebook \mathcal{C} :

$$Z_q = \mathbf{q}(Z_c) := \left(\arg \min_{c_k \in \mathcal{C}} \|Z_c^{(i,j)} - c_k\| \right) \in \mathbb{R}^{h \times w \times d}. \quad (1)$$

The final reconstruction result is obtained through:

$$\mathbf{I}_r = \mathcal{D}(\mathbf{Z}_q) = \mathcal{D}(\mathbf{q}(\mathcal{E}(\mathbf{I}_f))) \approx \mathbf{I}_f. \quad (2)$$

The indices sequence $s \in \{0, \dots, |\mathcal{C}| - 1\}^{hw}$ of \mathbf{Z}_c in codebook \mathcal{C} is defined as:

$$s^{(i,j)} = k \quad \text{such that} \quad \mathbf{Z}_q^{(i,j)} = c_k. \quad (3)$$

During pre-training, the above three modules (encoder \mathcal{E} , codebook \mathcal{C} , and decoder \mathcal{D}) can be optimized in an end-to-end manner. We follow VQGAN and adopt L1 loss \mathcal{L}_1 , perceptual loss \mathcal{L}_{per} (Johnson, Alahi, and Fei-Fei 2016; Zhang et al. 2018), and adversarial loss \mathcal{L}_{adv} (Esser, Rombach, and Ommer 2021) between the reconstructed image \mathbf{I}_r and the input \mathbf{I}_f . \mathcal{L}_{code} and commitment loss \mathcal{L}_{comm} are used to update the codebook \mathcal{C} and encoder \mathcal{E} , respectively:

$$\begin{aligned} \mathcal{L}_1 &= \|\mathbf{I}_f - \mathbf{I}_r\|_1, \\ \mathcal{L}_{per} &= \|\Phi(\mathbf{I}_f) - \Phi(\mathbf{I}_r)\|_2^2, \\ \mathcal{L}_{adv} &= -\log \mathcal{D}(\mathbf{I}_r), \\ \mathcal{L}_{code} &= \|\mathbf{sg}(\mathbf{Z}_c) - \mathbf{Z}_q\|_2^2, \\ \mathcal{L}_{comm} &= \|\mathbf{Z}_c - \mathbf{sg}(\mathbf{Z}_q)\|_2^2, \end{aligned} \quad (4)$$

where $\mathbf{sg}(\cdot)$ indicates the stop gradient operation. Φ denotes a pre-trained VGG16 model (Simonyan and Zisserman 2014) and \mathcal{D} represents the discriminator.

The overall training loss of VQGAN is summarized as:

$$\mathcal{L} = \mathcal{L}_1 + \mathcal{L}_{per} + \lambda_{adv}\mathcal{L}_{adv} + \mathcal{L}_{code} + \lambda_{comm}\mathcal{L}_{comm}. \quad (5)$$

λ_{comm} and λ_{adv} are the trade-off parameters and we set them to 0.5 and 0.8 in our experiment, respectively.

Notably, our VQGAN demonstrates remarkable generalization capabilities across out-of-domain glyphs and styles. As shown in Fig. 4, although these font styles and characters do not appear in the training process, nearly all stroke details are well reconstructed with the quantization process, showing the ability in generalizing to different font images.

3.2 Token Prior Refinement

To effectively integrate the token prior, VQ-Font leverages the well-trained codebook \mathcal{C} and decoder \mathcal{D} . It casts font generation task into indices prediction task. This process involves aggregating fine-grained styles from reference glyphs and predicting codebook indices of ground-truth glyph \mathbf{I}_g .

Styles aggregation. Following FS-Font, our VQ-Font employs a cross-attention module to attentively capture fine-grained styles, where it takes a content glyph \mathbf{I}_c as query, and k reference glyphs \mathbf{I}_S as key and value. Specifically, we first use a content encoder \mathcal{E}_c and a style encoder \mathcal{E}_s to extract the feature maps from \mathbf{I}_c and \mathbf{I}_S , i.e., $\mathbf{f}_c \in \mathbb{R}^{hw \times c}$ and $\mathbf{f}_S \in \mathbb{R}^{khw \times c}$. Then, we calculate their attention weights as:

$$\mathbf{A}_{patch} = \frac{(\mathbf{W}^Q \mathbf{f}_c)(\mathbf{W}^K \mathbf{f}_S)^T}{\sqrt{c}}, \quad (6)$$

where \mathbf{W}^Q and \mathbf{W}^K are learnable parameters to project the extracted features into query and key, respectively. c is set to

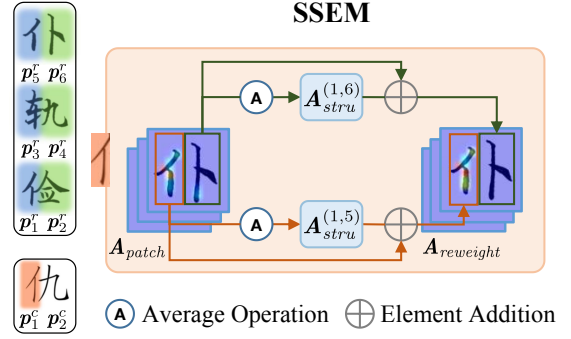


Figure 5: The overview of our Structure-level Style Enhancement Module (SSEM).

256. With the above weights, VQ-Font attentively captures patch-level styles from reference features \mathbf{f}_S to obtain the aggregated features \mathbf{f}_{cs} , which is formulated as:

$$\mathbf{f}_{cs} = \text{Softmax}(\mathbf{A}_{patch}) \cdot (\mathbf{W}^V \mathbf{f}_S), \quad (7)$$

In this way, we obtain patch-level aggregation features from the references, which may easily generate distorted strokes. Therefore, we need further fine-tuning for better quality.

Vector-Quantized font generation. To exploit the token prior in VQGAN, VQ-Font aims to quantize \mathbf{f}_{cs} into \mathbf{f}_q according to font codebook \mathcal{C} . However, due to the discrepancy between the feature spaces of \mathbf{f}_{cs} and the VQGAN encoded, it is infeasible to compute the indices sequence of \mathbf{f}_{cs} by nearest neighbor lookup. Inspired by (Zhou et al. 2022), we utilize a Transformer module to predict the indices $s_{cs} \in \{0, \dots, |\mathcal{C}| - 1\}^{hw}$ for all patch tokens of \mathbf{f}_{cs} . It employs 15 self-attention layers to globally model all tokens and an MLP to classify each token. Given the target glyph \mathbf{I}_g , we optimize this module from two aspects: (i) index prediction and (ii) image regression. Intuitively, the indices of \mathbf{f}_{cs} can be approximated to those indices obtained by encoding and quantizing ground-truth font \mathbf{I}_g . Moreover, a glyph image \mathbf{I}_g is projected from \mathbf{f}_q with the VQGAN decoder and is combined with \mathbf{I}_g to obtain reconstruction loss. To generalize the token prior to this task and preserve the effectiveness of prior knowledge, we fix the font codebook and only fine-tune the former layers of the decoder.

3.3 Structure-level Style Enhancement (SSEM)

Although leveraging the learned priors could promisingly improve the quality of synthesized glyphs, there are still inconsistent fine-grained styles between synthesized and reference glyphs, e.g., the last second row in Fig. 7. Compared to style transfer in RGB images, few-shot font generation in single-channel glyphs is more likely to acquire irrelevant patch-level styles. The main reason is that the original attention weights \mathbf{A}_{patch} are mainly based on geometry. To enhance the fidelity of captured styles, we propose to utilize the inherent structure (See Fig. 2) of Chinese characters to further recalibrate the attention weights.

Based on Fig. 2, we decompose the content glyph and reference glyphs into the structure components $\{\mathbf{p}_i^c\}_{i=0}^m$ and $\{\mathbf{p}_j^r\}_{j=0}^n$, where \mathbf{p}_i^c and \mathbf{p}_j^r denote the set of patch positions. After that, we calculate the structure-level attention weights $\mathbf{A}_{stru} \in \mathbb{R}^{m \times n}$. As illustrated in Fig. 5, the attention weight $\mathbf{A}_{stru}^{(i,j)}$ between \mathbf{p}_i^c and \mathbf{p}_j^r is obtained by averaging their corresponding patch-level weights:

$$\mathbf{A}_{stru}^{(i,j)} = \frac{1}{|\mathbf{p}_i^c| \cdot |\mathbf{p}_j^r|} \sum_{x \in \mathbf{p}_i^c, y \in \mathbf{p}_j^r} \mathbf{A}_{patch}^{(x,y)}. \quad (8)$$

Finally, we reweight \mathbf{A}_{patch} by adding \mathbf{A}_{stru} to the corresponding patch positions:

$$\mathbf{A}_{reweight} = \mathbf{A}_{patch} \oplus \mathbf{A}_{stru}. \quad (9)$$

The new fusion feature \mathbf{f}_{cs} in Eqn. (7) is reformulated as:

$$\mathbf{f}_{cs}^* = \text{Softmax}(\mathbf{A}_{reweight}) \cdot (\mathbf{W}^V \mathbf{f}_S). \quad (10)$$

In this way, our attention map can concentrate more on matching corresponding structure components, and reduce the adverse effect of other irrelevant strokes. Fig. 8 shows that after SSEM, our attention map $\mathbf{A}_{reweight}$ has higher attention in corresponding structure components, thereby benefiting the following style transformation.

3.4 Training Objective

We train the content encoder \mathcal{E}_c , style encoder \mathcal{E}_s , cross-attention module, and Transformer module using cross-entropy loss \mathcal{L}_{indice} while keeping font codebook fixed. We fine-tune the first four layers of the pre-trained font decoder using VQGAN-like losses, including L1 loss \mathcal{L}_1 , perceptual loss \mathcal{L}_{per} , and adversarial loss \mathcal{L}_{adv} .

Cross Entropy loss. We first obtain the ground-truth codebook indices \mathbf{s}_g using Eqn. (3) by taking the ground-truth font image \mathbf{I}_g into the pre-trained VQGAN. To further improve the prediction performance, we follow FS-Font and design a self-reconstruction branch that uses \mathbf{I}_g as the reference glyph. The code indices learning is defined as:

$$\mathcal{L}_{indice}^{main} = \text{CE}(\hat{\mathbf{s}}_{cs}, \mathbf{s}_g); \quad \mathcal{L}_{indice}^{self} = \text{CE}(\tilde{\mathbf{s}}_{cs}, \mathbf{s}_g), \quad (11)$$

where $\hat{\mathbf{s}}_{cs}$ represents the indices predicted by the main branch and $\tilde{\mathbf{s}}_{cs}$ represents the indices predicted by the self-reconstruction branch.

L1 loss. To maintain pixel-level consistency between the generated font images \mathbf{I}_q and the ground-truth font images \mathbf{I}_g , we employ L1 loss as our reconstruction loss:

$$\mathcal{L}_1^f = \|\mathbf{I}_g - \mathbf{I}_q\|_1. \quad (12)$$

Adversarial loss and Perceptual loss. To further ensure that the generated font images have high visual quality, we additionally utilize adversarial loss and perceptual loss. Moreover, in our experiments, we employ a multi-head projection discriminator (Park et al. 2021a) and use the Unicode encoding of each Chinese character as the label:

$$\begin{aligned} \mathcal{L}_{adv}^D &= -\mathbb{E}_{\mathbf{I}_g \sim p_{data}} \max(0, -1 + D_{uni}(\mathbf{I}_g)) \\ &\quad -\mathbb{E}_{\mathbf{I}_q \sim p_{gen}} \max(0, -1 - D_{uni}(\mathbf{I}_q)), \\ \mathcal{L}_{adv}^G &= -\mathbb{E}_{\mathbf{I}_q \sim p_{gen}} D_{uni}(\mathbf{I}_q), \\ \mathcal{L}_{per}^f &= \|\Phi(\mathbf{I}_g) - \Phi(\mathbf{I}_q)\|_2^2, \end{aligned} \quad (13)$$

where Φ denotes VGG16 same as that in Eqn. (4).

Overall objective loss. To sum up, the final loss function for training our VQ-Font is formulated as:

$$\begin{aligned} \mathcal{L}_{VQ-Font} &= \lambda_{self} \mathcal{L}_{indice}^{self} + \lambda_{main} \mathcal{L}_{indice}^{main} + \lambda_1^f \mathcal{L}_1^f \\ &\quad + \lambda_{adv}^f \mathcal{L}_{adv}^G + \lambda_{per}^f \mathcal{L}_{per}^f, \end{aligned} \quad (14)$$

where λ_{self} , λ_{main} , λ_1^f , λ_{adv}^f and λ_{per}^f are the trade-off parameters for balancing each loss item. In our experiments, we set $\lambda_{main} = \lambda_1^f = 2$, $\lambda_{self} = \lambda_{per}^f = 1$ and $\lambda_{adv}^f = 0.002$.

4 Experiments

4.1 Datasets and Evaluation Metrics

We follow previous works (Park et al. 2021a,b; Tang et al. 2022) and collect 382 fonts with various types to build our dataset. Each font contains 3499 Chinese characters and the resolution for each character is 128×128 . We split these 3499 characters into 3 groups, *i.e.*, 2841 seen characters, 158 reference characters, and 500 unseen characters. For each character, we follow FS-Font (Tang et al. 2022) and select 3 reference characters from the reference set that can cover most of its structure components. We use Kai font as our default content font and train our model on 371 seen fonts, leaving 10 unseen fonts that do not appear in the training stage. In this way, our training set totally consists of 371 seen fonts, each of which has 2841 seen characters (SFSC). Our test set consists of two parts, *i.e.*, 10 seen fonts with 500 unseen characters (SFUC) and 10 unseen fonts with 500 unseen characters (UFUC), encompassing a diverse range of font types, such as handwriting, printing, and artistic styles.

To evaluate the performance, we follow these competing methods and report the L1, RMSE, PSNR, SSIM and LPIPS (Zhang et al. 2018), covering both pixel consistency and perceptual similarity. Additionally, we also conduct a user study to further assess the visual quality of the generated results from human perception.

4.2 Implementation Details

In the pre-training phase of our font codebook, we encode the font images into 16×16 features. The size of our font codebook is set to 1,024. At this stage, VQGAN is trained for $2e5$ iterations with a learning rate of $4e-5$. The number of attention heads in the cross-attention module is set to 8. We select 3 reference characters for each Chinese character. In the subsequent token prior refinement stage, we keep the pre-trained font codebook and the later layers of the decoder fixed, while concentrating on training the remaining layers of the VQ-Font for 300k iterations. Here, the learning rate is set to $2e-4$. We adopt Adam optimizer (Kingma and Ba 2014) with a batch size of 32 and rely on one A6000 GPU.

4.3 Comparison Methods

We compare the performance of our proposed VQ-Font with five state-of-the-art methods, including LF-Font (Park et al. 2021a), MX-Font (Park et al. 2021b), DG-Font (Xie et al. 2021), FS-Font (Tang et al. 2022), and CF-Font (Wang et al. 2023). To make a fair comparison, we retrain all these methods using their default settings on our dataset. More results and analyses can be found in our suppl.

Seen Fonts Unseen Chars (SFUC)							
Method	L1 ↓	RMSE ↓	PSNR ↑	SSIM ↑	LPIPS ↓	User (C)% ↑	User (S)% ↑
LF-Font (AAAI 2021)	0.0921	0.264	17.818	0.746	0.157	70.5	4.0
MX-Font (ICCV 2021)	0.1002	0.278	17.326	0.725	0.169	83.4	2.9
DG-Font (CVPR 2021)	0.0747	0.233	18.901	0.782	0.127	80.7	6.7
FS-Font (CVPR 2022)	<u>0.0663</u>	0.220	<u>19.702</u>	<u>0.805</u>	0.126	90.3	<u>12.9</u>
CF-Font (CVPR 2023)	0.0667	<u>0.217</u>	19.559	<u>0.805</u>	<u>0.111</u>	86.7	10.6
VQ-Font (Ours)	0.0610	0.209	20.285	0.822	0.096	97.2	62.9

Unseen Fonts Unseen Chars (UFUC)							
Method	L1 ↓	RMSE ↓	PSNR ↑	SSIM ↑	LPIPS ↓	User (C)% ↑	User (S)% ↑
LF-Font (AAAI 2021)	0.0976	0.274	17.495	0.726	0.174	68.0	3.4
MX-Font (ICCV 2021)	0.1061	0.288	17.045	0.706	0.185	76.5	4.0
DG-Font (CVPR 2021)	0.0807	0.246	18.465	0.768	0.139	78.4	4.7
FS-Font (CVPR 2022)	<u>0.0666</u>	<u>0.220</u>	<u>19.672</u>	0.797	0.137	<u>84.5</u>	9.2
CF-Font (CVPR 2023)	0.0685	0.222	19.344	<u>0.798</u>	<u>0.116</u>	84.3	<u>11.3</u>
VQ-Font (Ours)	0.0621	0.210	20.249	0.812	0.103	95.6	67.4

Table 1: Quantitative comparison with state-of-the-art methods on SFUC and UFUC datasets.

Content	铃 杖 竿 窄 匪	纒 涯 贛 宴 亏	肢 驻 牢 遍 衙	豺 阻 冤 丑 喻	渔 缀 譬 毫 间
LF-Font	铃 杖 竿 窄 匪	纒 涯 贛 宴 亏	肢 驻 牢 遍 衙	豺 阻 冤 丑 喻	渔 缀 譬 毫 间
MX-Font	铃 杖 竿 窄 匪	纒 涯 贛 宴 亏	肢 驻 牢 遍 衙	豺 阻 冤 丑 喻	渔 缀 譬 毫 间
DG-Font	铃 杖 竿 窄 匪	纒 涯 贛 宴 亏	肢 驻 牢 遍 衙	豺 阻 冤 丑 喻	渔 缀 譬 毫 间
FS-Font	铃 杖 竿 窄 匪	纒 涯 贛 宴 亏	肢 驻 牢 遍 衙	豺 阻 冤 丑 喻	渔 缀 譬 毫 间
CF-Font	铃 杖 竿 窄 匪	纒 涯 贛 宴 亏	肢 驻 牢 遍 衙	豺 阻 冤 丑 喻	渔 缀 譬 毫 间
VQ-Font	铃 杖 竿 窄 匪	纒 涯 贛 宴 亏	肢 驻 牢 遍 衙	豺 阻 冤 丑 喻	渔 缀 譬 毫 间
Target	铃 杖 竿 窄 匪	纒 涯 贛 宴 亏	肢 驻 牢 遍 衙	豺 阻 冤 丑 喻	渔 缀 譬 毫 间

Figure 6: Qualitative comparison with competing methods on UFUC dataset. Best view it by zooming in on the screen.

Quantitative evaluation. Tab. 1 presents the comparison of our VQ-Font with other state-of-the-art methods. The results demonstrate that our approach outperforms others in terms of both pixel-based and perception-based metrics on UFUC and SFUC datasets. Specifically, in terms of L1, we obtain 7.99% improvement over the second-best result on SFUC dataset and 6.76% on UFUC dataset, respectively. As for LPIPS, our VQ-Font outperforms the second-best result with a large margin, *i.e.*, 13.51% improvement on SFUC dataset and 11.21% improvement on UFUC dataset. This indicates that the synthesized results of our VQ-Font have a better fidelity and also align better with human perception.

Qualitative evaluation. As shown in Fig. 6, we select various styles of fonts, including serif, artistic, and handwriting fonts, from UFUC dataset for qualitative comparison. We can observe that LF-font and MX-font struggle to capture the fine-grained styles, resulting in stroke artifacts (see red boxes). DG-Font and CF-Font also exhibit missing

strokes and distorted strokes in challenging cases (*e.g.*, 2~3 columns in Fig. 6). Besides, FS-Font tends to produce blurry font and lose stroke details (*e.g.*, 5~6 columns in Fig. 6). In comparison, our proposed VQ-Font can effectively capture and transfer the stroke-level and structure-level styles of the reference glyphs. The integration of token prior further contributes to the higher quality of the glyphs.

User study. To further compare the visual quality of different methods, we conduct a user study. A total of 30 volunteers with computer vision backgrounds participated in evaluating the experimental results. We utilize 10 fonts with challenging styles (*e.g.*, 2~4 columns in Fig. 6) in UFUC and SFUC datasets respectively, and randomly generate 10 characters for each font using these methods. Here we consider two items, *i.e.*, 1) content accuracy which classifies whether the font images within each method have extra strokes and other anomalies or not, and 2) style consistency which concentrates on selecting the font images among all

	L1 ↓	RMSE ↓	PSNR ↑	SSIM ↑	LPIPS ↓
Baseline	0.0678	0.223	19.318	0.793	0.116
+C	0.0628	0.212	20.170	0.810	0.105
+CS	0.0621	0.210	20.249	0.812	0.103

Table 2: **Quantitative results of different VQ-Font variants.** C and S represent codebook and SSEM, respectively.

Content	辉	帜	耙	阳	肌	遍
Reference						
Baseline						
+C						
+CS						
Target						

Figure 7: **Qualitative results of different VQ-Font variants.** The structure components appearing in the reference glyphs are highlighted with blue boxes.

the methods that are closest to the reference in stroke style, stroke thickness, and edge details. The evaluation result on the right part of Tab. 1 demonstrates that on the one hand, our method has better content accuracy than others from human perception. On the other hand, users are more likely to select our results which have better style consistency, while other methods struggle with these challenging font styles.

4.4 Ablation Study

In this section, we mainly discuss the effectiveness of token prior refinement and structure-aware enhancement. We first train a baseline model by utilizing the cross-attention mechanism to learn the spatial correspondence at the patch level which is similar to FS-Font. Then, we gradually add the pre-trained font codebook and structure-level style enhancement module (SSEM) to the baseline for validation. Tab. 2 shows the quantitative results on UFUC. One can see that the pre-trained font codebook (+C) can obviously improve the SSIM and LPIPS performance, which indicates the better visual quality brought by our font codebook. When combining the codebook with the structure-level style enhancement module (+CS), our method has a further improvement, especially in PSNR. This indicates that SSEM can effectively capture the reference styles and contribute to higher fidelity.

The visual comparison in Fig. 7 demonstrates a noticeable reduction in distorted strokes and missing details when utilizing the font codebook (+C). Besides, our SSEM enhances the fidelity of the generated glyphs by aligning them more accurately with the corresponding structure components in the reference. These improved regions are high-

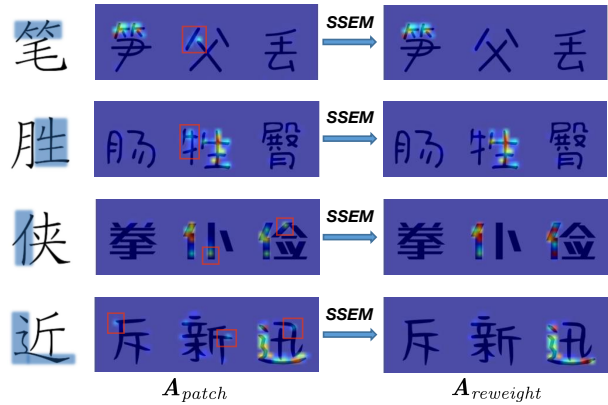


Figure 8: **Attention maps w/o and w/ SSEM.**

Decoder	L1 ↓	RMSE ↓	PSNR ↑	SSIM ↑	LPIPS ↓
Fix	0.0648	0.216	20.069	0.805	0.121
Fine-tune	0.0621	0.210	20.249	0.812	0.103

Table 3: **Comparison of fixed and fine-tuned decoders.**

lighted within the blue box. Both the quantitative and qualitative evaluations demonstrate the improvements in fidelity and visual quality brought by our token prior refinement and structure-aware enhancement.

To further validate the effectiveness of SSEM, we visualize the attention maps before and after enhancement operation. As shown in Fig. 8, the leftmost column represents the content glyphs, and the visualized components are highlighted in blue. The visualization of different structure components demonstrates that our enhancement operation can eliminate the attention on irrelevant regions (see red boxes) and concentrate more on the corresponding components of the reference. This helps to capture the structure-level styles and then boosts the subsequent style transformation.

Finally, we explore the effect of fine-tuning the pre-trained font decoder in our method. We conduct another experiment by freezing all parameters of the decoder. From Tab. 3 we can see that although the pre-trained decoder has the ability to generate photo-realistic font images, by fine-tuning the decoder with the end-to-end optimization, it can well generalize to our font generation task and bridge the domain gap between our synthetic and real-world fonts.

5 Conclusion

In this paper, we propose VQ-Font, a new few-shot font generation framework. It refines the font images by incorporating token prior encapsulated in a pre-trained font codebook. Additionally, the Structure-level Style Enhancement Module (SSEM) leverages the structure information of Chinese characters to recalibrate fine-grained styles from the references. This enhances the alignment of structure-level styles between content and reference glyphs. By combining the token prior refinement and SSEM, the results of our VQ-Font are more realistic and have higher fidelity in comparison with other start-of-the-art methods.

References

- Cha, J.; Chun, S.; Lee, G.; Lee, B.; Kim, S.; and Lee, H. 2020. Few-shot compositional font generation with dual memory. In *European Conference on Computer Vision*, 735–751. Springer.
- Chang, J.; Gu, Y.; Zhang, Y.; Wang, Y.-F.; and Innovation, C. 2018. Chinese Handwriting Imitation with Hierarchical Generative Adversarial Network. In *BMVC*, 290.
- Chen, C.; Shi, X.; Qin, Y.; Li, X.; Han, X.; Yang, T.; and Guo, S. 2022. Real-world blind super-resolution via feature matching with implicit high-resolution priors. In *Proceedings of the 30th ACM International Conference on Multimedia*, 1329–1338.
- Esser, P.; Rombach, R.; and Ommer, B. 2021. Taming transformers for high-resolution image synthesis. In *IEEE Conference on Computer Vision and Pattern Recognition*, 12873–12883.
- Fu, B.; He, J.; Wang, J.; and Qiao, Y. 2023. Neural Transformation Fields for Arbitrary-Styled Font Generation. In *IEEE Conference on Computer Vision and Pattern Recognition*, 22438–22447.
- Gao, Y.; Guo, Y.; Lian, Z.; Tang, Y.; and Xiao, J. 2019. Artistic glyph image synthesis via one-stage few-shot learning. *ACM Transactions on Graphics (TOG)*, 38(6): 1–12.
- Gao, Y.; and Wu, J. 2020. Gan-based unpaired chinese character image translation via skeleton transformation and stroke rendering. In *proceedings of the AAAI conference on artificial intelligence*, volume 34, 646–653.
- Gu, Y.; Wang, X.; Xie, L.; Dong, C.; Li, G.; Shan, Y.; and Cheng, M.-M. 2022. VQFR: Blind face restoration with vector-quantized dictionary and parallel decoder. In *European Conference on Computer Vision*, 126–143. Springer.
- Hassan, A. U.; Ahmed, H.; and Choi, J. 2021. Unpaired font family synthesis using conditional generative adversarial networks. *Knowledge-Based Systems*, 229: 107304.
- Hinton, G. E.; and Zemel, R. 1993. Autoencoders, minimum description length and Helmholtz free energy. *Advances in neural information processing systems*, 6.
- Isola, P.; Zhu, J.-Y.; Zhou, T.; and Efros, A. A. 2017. Image-to-image translation with conditional adversarial networks. In *IEEE Conference on Computer Vision and Pattern Recognition*, 1125–1134.
- Jiang, Y.; Lian, Z.; Tang, Y.; and Xiao, J. 2017. DCFont: an end-to-end deep Chinese font generation system. In *SIGGRAPH Asia 2017 Technical Briefs*, 1–4.
- Jiang, Y.; Lian, Z.; Tang, Y.; and Xiao, J. 2019. Sfont: Structure-guided chinese font generation via deep stacked networks. In *Proceedings of the AAAI conference on artificial intelligence*, volume 33, 4015–4022.
- Johnson, J.; Alahi, A.; and Fei-Fei, L. 2016. Perceptual losses for real-time style transfer and super-resolution. In *European Conference on Computer Vision*, 694–711. Springer.
- Karras, T.; Laine, S.; Aittala, M.; Hellsten, J.; Lehtinen, J.; and Aila, T. 2020. Analyzing and improving the image quality of StyleGAN. In *IEEE Conference on Computer Vision and Pattern Recognition*.
- Kingma, D. P.; and Ba, J. 2014. Adam: A method for stochastic optimization. *arXiv preprint arXiv:1412.6980*.
- Li, X.; Zuo, W.; and Loy, C. C. 2023. Learning Generative Structure Prior for Blind Text Image Super-resolution. In *IEEE Conference on Computer Vision and Pattern Recognition*.
- Liu, W.; Liu, F.; Ding, F.; He, Q.; and Yi, Z. 2022. Xmp-font: self-supervised cross-modality pre-training for few-shot font generation. In *IEEE Conference on Computer Vision and Pattern Recognition*, 7905–7914.
- Lyu, P.; Bai, X.; Yao, C.; Zhu, Z.; Huang, T.; and Liu, W. 2017. Auto-encoder guided GAN for Chinese calligraphy synthesis. In *2017 14th IAPR International Conference on Document Analysis and Recognition (ICDAR)*, volume 1, 1095–1100. IEEE.
- Park, S.; Chun, S.; Cha, J.; Lee, B.; and Shim, H. 2021a. Few-shot font generation with localized style representations and factorization. In *Proceedings of the AAAI conference on artificial intelligence*, volume 35, 2393–2402.
- Park, S.; Chun, S.; Cha, J.; Lee, B.; and Shim, H. 2021b. Multiple heads are better than one: Few-shot font generation with multiple localized experts. In *IEEE International Conference on Computer Vision*, 13900–13909.
- Razavi, A.; Van den Oord, A.; and Vinyals, O. 2019. Generating diverse high-fidelity images with vq-vae-2. *Advances in neural information processing systems*, 32.
- Simonyan, K.; and Zisserman, A. 2014. Very deep convolutional networks for large-scale image recognition. *arXiv preprint arXiv:1409.1556*.
- Sun, D.; Ren, T.; Li, C.; Su, H.; and Zhu, J. 2017. Learning to write stylized chinese characters by reading a handful of examples. *arXiv preprint arXiv:1712.06424*.
- Sun, D.; Zhang, Q.; and Yang, J. 2018. Pyramid embedded generative adversarial network for automated font generation. In *2018 24th International Conference on Pattern Recognition (ICPR)*, 976–981. IEEE.
- Tang, L.; Cai, Y.; Liu, J.; Hong, Z.; Gong, M.; Fan, M.; Han, J.; Liu, J.; Ding, E.; and Wang, J. 2022. Few-shot font generation by learning fine-grained local styles. In *IEEE Conference on Computer Vision and Pattern Recognition*, 7895–7904.
- Tian, Y. 2016. Rewrite: Neural style transfer for chinese fonts, 2016. Retrieved Nov, 23: 2016.
- Tian, Y. 2017. Master Chinese calligraphy with conditional adversarial networks.
- Van Den Oord, A.; Vinyals, O.; et al. 2017. Neural discrete representation learning. *Advances in neural information processing systems*, 30.
- Vaswani, A.; Shazeer, N.; Parmar, N.; Uszkoreit, J.; Jones, L.; Gomez, A. N.; Kaiser, Ł.; and Polosukhin, I. 2017. Attention is all you need. *Advances in neural information processing systems*, 30.
- Wang, C.; Zhou, M.; Ge, T.; Jiang, Y.; Bao, H.; and Xu, W. 2023. CF-Font: Content Fusion for Few-shot Font Generation. In *IEEE Conference on Computer Vision and Pattern Recognition*, 1858–1867.

Wen, C.; Pan, Y.; Chang, J.; Zhang, Y.; Chen, S.; Wang, Y.; Han, M.; and Tian, Q. 2021. Handwritten Chinese font generation with collaborative stroke refinement. In *Proceedings of the IEEE/CVF Winter Conference on Applications of Computer Vision*, 3882–3891.

Wu, R.-Q.; Duan, Z.-P.; Guo, C.-L.; Chai, Z.; and Li, C. 2023. RIDCP: Revitalizing Real Image Dehazing via High-Quality Codebook Priors. In *IEEE Conference on Computer Vision and Pattern Recognition*, 22282–22291.

Wu, S.-J.; Yang, C.-Y.; and Hsu, J. Y.-j. 2020. Calligan: Style and structure-aware chinese calligraphy character generator. *arXiv preprint arXiv:2005.12500*.

Xie, Y.; Chen, X.; Sun, L.; and Lu, Y. 2021. Dg-font: Deformable generative networks for unsupervised font generation. In *IEEE Conference on Computer Vision and Pattern Recognition*, 5130–5140.

Yang, S.; Liu, J.; Wang, W.; and Guo, Z. 2019a. Tet-gan: Text effects transfer via stylization and destylization. In *Proceedings of the AAAI Conference on Artificial Intelligence*, volume 33, 1238–1245.

Yang, S.; Wang, Z.; Wang, Z.; Xu, N.; Liu, J.; and Guo, Z. 2019b. Controllable artistic text style transfer via shape-matching gan. In *IEEE International Conference on Computer Vision*, 4442–4451.

Zhang, R.; Isola, P.; Efros, A. A.; Shechtman, E.; and Wang, O. 2018. The unreasonable effectiveness of deep features as a perceptual metric. In *IEEE Conference on Computer Vision and Pattern Recognition*, 586–595.

Zhang, Y.; Zhang, Y.; and Cai, W. 2018. Separating style and content for generalized style transfer. In *IEEE Conference on Computer Vision and Pattern Recognition*, 8447–8455.

Zhou, S.; Chan, K.; Li, C.; and Loy, C. C. 2022. Towards robust blind face restoration with codebook lookup transformer. *Advances in Neural Information Processing Systems*, 35: 30599–30611.

A Supplementary Material

In the supplementary material, we first introduce the architecture of Transformer module used for predicting the glyph indices. Then, we analyze the impact of font codebook size on the generated font images. Next, we describe how we partition Chinese characters into structure components with structure-level style enhancement module. Finally, we present additional font generation results and examples of different Chinese character structures.

A.1 Transformer Module

As shown in Fig. 9, our Transformer module consists of a total of 15 blocks, where each block includes a multi-head self-attention module and a feed-forward network (FFN). The input for the first block is the fusion feature f_{cs}^* , while the remaining blocks receive the output of the previous block as their input. We set the number of the attention head to 8 in the multi-head self-attention module. Furthermore, we incorporate learnable positional embeddings (PE) on Keys and Queries. These positional embeddings provide spatial information and help the model understand the relative positions of different patches within f_{cs}^* . To obtain the indices sequence s_{cs} corresponding to the target glyph, we input f_{cs}^* aggregating both patch-level and structure-level styles into the Transformer module and subsequently an MLP (Multi-Layer Perceptron) is employed to classify each token. By replacing s_{cs} with the discrete codes of the codebook, our method can effectively encapsulate the token prior to the synthesized glyphs.

A.2 Impact of Font Codebook Size

In our model, the font codebook plays a crucial role that makes the synthesized glyphs more closely to the real-world glyphs and reduces the occurrence of distorted strokes. Inspired by previous works (Chen et al. 2022; Zhou et al. 2022; Gu et al. 2022; Li, Zuo, and Loy 2023; Wu et al. 2023), the size of the codebook affects the overall expressive capability. To investigate this in our model, we conduct an ablation study on the size of the font codebook. During the experiments, we set the codebook size to 128, 512, and 1024, while keeping other model settings consistent. We employ L1, RMSE, PSNR, SSIM, and LPIPS (Zhang et al. 2018) as metrics to quantify the experimental results on UFUC dataset. With the increase of the size, font codebook encapsulates richer token prior. From the results presented in Tab. 4, it can be observed that the model achieves the best performance when the codebook size is set to 1024.

	L1 ↓	RMSE ↓	PSNR ↑	SSIM ↑	LPIPS ↓
128	0.0638	0.214	20.010	0.807	0.108
512	0.0631	0.212	20.074	0.809	0.107
1024	0.0621	0.210	20.249	0.812	0.103

Table 4: Effect of different codebook sizes when pre-training VQGAN.

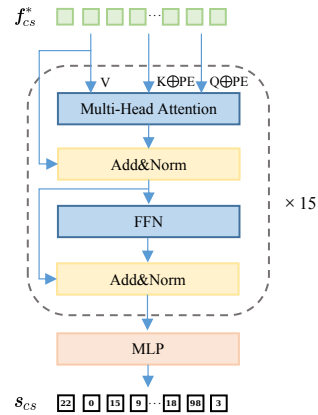


Figure 9: The illustration of the Transformer module.

A.3 Chinese Character Partition in SSEM

In the structure-level style enhancement module (SSEM), we explicitly divide the Chinese characters with various structures to obtain the structural-level styles. Next, we will briefly describe our approach.

In Chinese characters, each character belongs to a specific structure. Shown in Fig. 10, Chinese characters can be divided into 12 different structure categories. Within each structure, the structure components are arranged according to the same paradigm. This uniformity in structure allows us to explicitly decompose Chinese characters into structure components. In our experiment, we first add structure labels to each character utilized. Then, we apply the same method of division to Chinese characters that belong to the same structure.

Taking the left-right arrangement and bottom-left encompassed structures as examples, as shown in Fig. 11, we partition the 16×16 feature maps into structure components based on the structure information of the characters. The remaining 10 structures are partitioned in a similar manner. Thus, we can obtain the position sets of different structure component patches. Consequently, utilizing the obtained position sets, we can locate the structure components of the content glyphs and style glyphs separately in $A_{patch} \in \mathbb{R}^{hw \times khw}$, where hw and khw represent the resolution of the content feature maps and the style feature maps respectively. By averaging the weights in the corresponding position sets of the content and style feature maps, we can obtain structure-level attention weight A_{stru} .

A.4 More Visual Results

As shown in Fig. 12, we show additional comparison results with existing state-of-the-art methods (LF-Font (Park et al. 2021a), MX-Font (Park et al. 2021b), DG-Font (Xie et al. 2021), FS-Font (Tang et al. 2022), and CF-Font (Wang et al. 2023).) on SFUC dataset. From the results, it is evident that the glyphs generated by our VQ-FONT effectively address the issue of distorted strokes.

As depicted in Figs. 13 and 14, we present additional experimental results on the test dataset including some chal-



Figure 10: Examples of Chinese characters with different structures.

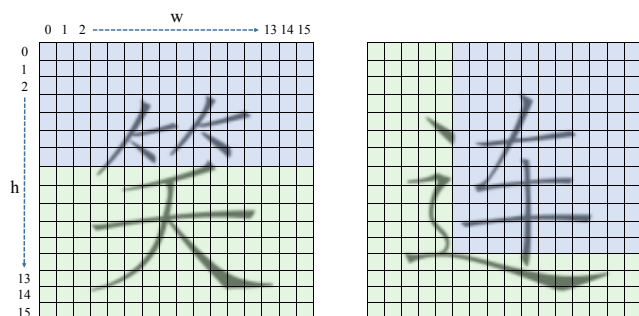


Figure 11: Different colors represent the position sets of different structure components in the feature map. Each small square represents a patch of the feature map.

lenging fonts. Our model exhibits good generalization performance, allowing it to generate glyphs across a wide range of styles with impressive results.

A.5 Examples of Different Structures

Chinese characters can be categorized into the following structures: left-right arrangement, left-center-right arrangement, top-bottom arrangement, top-center-bottom arrangement, fully encompassed, top-three encompassed, left-three encompassed, bottom-three encompassed, top-left encompassed, top-right encompassed, bottom-left encompassed, and independent structure. As shown in Fig. 10, we provide several Chinese characters for each structure.

Content	径 锯 倔 监 闰	饰 揭 蝠 扁 逗	枯 讯 杏 罢 开
LF-Font	径 锯 倔 监 闰	饰 揭 蝠 扁 逗	枯 讯 杏 罢 开
MX-Font	径 锯 倔 监 闰	饰 揭 蝠 扁 逗	枯 讯 杏 罢 开
DG-Font	径 锯 倔 监 闰	饰 揭 蝠 扁 逗	枯 讯 杏 罢 开
FS-Font	径 锯 倔 监 闰	饰 揭 蝠 扁 逗	枯 讯 杏 罢 开
CF-Font	径 锯 倔 监 闰	饰 揭 蝠 扁 逗	枯 讯 杏 罢 开
VQ-Font	径 锯 倔 监 闰	饰 揭 蝠 扁 逗	枯 讯 杏 罢 开
Target	径 锯 倔 监 闰	饰 揭 蝠 扁 逗	枯 讯 杏 罢 开
Content	湘 涯 康 夯 昆	绢 棍 罢 箍 朱	泣 拆 述 嫁 丑
LF-Font	湘 涯 康 夯 昆	绢 棍 罢 箍 朱	泣 拆 述 嫁 丑
MX-Font	湘 涯 康 夯 昆	绢 棍 罢 箍 朱	泣 拆 述 嫁 丑
DG-Font	湘 涯 康 夯 昆	绢 棍 罢 箍 朱	泣 拆 述 嫁 丑
FS-Font	湘 涯 康 夯 昆	绢 棍 罢 箍 朱	泣 拆 述 嫁 丑
CF-Font	湘 涯 康 夯 昆	绢 棍 罢 箍 朱	泣 拆 述 嫁 丑
VQ-Font	湘 涯 康 夯 昆	绢 棍 罢 箍 朱	泣 拆 述 嫁 丑
Target	湘 涯 康 夯 昆	绢 棍 罢 箍 朱	泣 拆 述 嫁 丑

Figure 12: Qualitative comparison with competing methods on SFUC dataset. Best view it by zooming in on the screen.

Content	阻寻掐天钉痰招芬组带耙监喊告旨搏赖色
Ours	阻寻掐天钉痰招芬组带耙监喊告旨搏赖色
Target	阻寻掐天钉痰招芬组带耙监喊告旨搏赖色
Content	仔搏兵但叭喝典瞧戏讯待善柒棍跟怕矿狗
Ours	仔搏兵但叭喝典瞧戏讯待善柒棍跟怕矿狗
Target	仔搏兵但叭喝典瞧戏讯待善柒棍跟怕矿狗
Content	律豺杏恤赴饶忱慎会检割让捺乡译辟沧辜丐拆
Ours	律豺杏恤赴饶忱慎会检割让捺乡译辟沧辜丐拆
Target	律豺杏恤赴饶忱慎会检割让捺乡译辟沧辜丐拆
Content	敌详咖针缀何族栏毫杰伞析窗匆棍悬检捺
Ours	敌详咖针缀何族栏毫杰伞析窗匆棍悬检捺
Target	敌详咖针缀何族栏毫杰伞析窗匆棍悬检捺
Content	铝倒童葵开拍则术跌罢析毫谜莫籽针埋膛
Ours	铝倒童葵开拍则术跌罢析毫谜莫籽针埋膛
Target	铝倒童葵开拍则术跌罢析毫谜莫籽针埋膛
Content	掉姚苟间吹述况辑俗赏渔何族仔荚胀杖汗
Ours	掉姚苟间吹述况辑俗赏渔何族仔荚胀杖汗
Target	掉姚苟间吹述况辑俗赏渔何族仔荚胀杖汗
Content	疗梯拿乔邻修啃很肢卑欢挤渗弃奄迈亥梨
Ours	疗梯拿乔邻修啃很肢卑欢挤渗弃奄迈亥梨
Target	疗梯拿乔邻修啃很肢卑欢挤渗弃奄迈亥梨
Content	驻盼共吆坚邑蝠费臊匀愉坎芝钩裙石枯榕
Ours	驻盼共吆坚邑蝠费臊匀愉坎芝钩裙石枯榕
Target	驻盼共吆坚邑蝠费臊匀愉坎芝钩裙石枯榕

Figure 13: The visual results of various fonts on SFUC dataset.

Content	跌后辣罢析纽县巫搓色莢主纯怕滥园彼让
Ours	跌后辣罢析纽县巫搓色莢主纯怕滥园彼让
Target	跌后辣罢析纽县巫搓色莢主纯怕滥园彼让
Content	而寄饰划慈交郁轧脏说星毡顽律浓揸卫杏
Ours	而寄饰划慈交郁轧脏说星毡顽律浓揸卫杏
Target	而寄饰划慈交郁轧脏说星毡顽律浓揸卫杏
Content	浑历捅供配肌阴骄阳牌众十倔齐互绢径走
Ours	浑历捅供配肌阴骄阳牌众十倔齐互绢径走
Target	浑历捅供配肌阴骄阳牌众十倔齐互绢径走
Content	拆畔栅涯彼崎邢彤崩伊衙挂伞闰吹掉呻劳县
Ours	拆畔栅涯彼崎邢彤崩伊衙挂伞闰吹掉呻劳县
Target	拆畔栅涯彼崎邢彤崩伊衙挂伞闰吹掉呻劳县
Content	叭讯柒矿驻蝠费匀坎钩裙枯室错洪册所秩
Ours	叭讯柒矿驻蝠费匀坎钩裙枯室错洪册所秩
Target	叭讯柒矿驻蝠费匀坎钩裙枯室错洪册所秩
Content	问匪尼讳愁羔亏孔蚂免牢淀谒驶哨秆叭遗
Ours	问匪尼讳愁羔亏孔蚂免牢淀谒驶哨秆叭遗
Target	问匪尼讳愁羔亏孔蚂免牢淀谒驶哨秆叭遗
Content	莫呐蒲辑俗赏渔敌撑详奖咖针缀何族膛栏
Ours	莫呐蒲辑俗赏渔敌撑详奖咖针缀何族膛栏
Target	莫呐蒲辑俗赏渔敌撑详奖咖针缀何族膛栏
Content	庠蛛往戈堆棕柱浅磅河故封姨夯吊奸挫疆
Ours	庠蛛往戈堆棕柱浅磅河故封姨夯吊奸挫疆
Target	庠蛛往戈堆棕柱浅磅河故封姨夯吊奸挫疆

Figure 14: The visual results of various fonts on UFUC dataset.